

FATIGUE 93

Volume III

**Editors J. - P. Bailon and J. I.
Dickson**

**Proceedings of the Fifth International
Conference on Fatigue and Fatigue
Thresholds held 3-7 May 1993
Montreal, Quebec, Canada.**

EFFECTS OF LOAD RATIO AND GASEOUS ENVIRONMENT ON NEAR-THRESHOLD
FATIGUE CRACK GROWTH IN A NiCrMoV ROTOR STEEL

J. Denk*, O.E.Lepik** and G.Ebi*

The near-threshold fatigue crack growth behaviour of material taken from a failed Darlington NGS Unit 2 generator rotor shaft was investigated. At low R-ratios a significant influence of environment and temperature was observed on the fatigue threshold. At high R-ratios the influence of environment and temperature disappeared and a threshold value of 2.8 MPa√m was measured. At negative R-ratios the fatigue threshold values were affected by the test procedure. High initial compressive loads during the test reduced the threshold value. This is attributed to a reduced closure level resulting from increased flattening of the fracture surfaces. For positive and negative R-ratios a lower bound effective fatigue threshold curve can be defined and used to establish NDE requirements.

INTRODUCTION

In March of 1990, during commissioning of Darlington Unit 2 NGS, excessive shaft vibrations led to the discovery of a crack in the generator rotor shaft. Subsequent metallurgical investigations revealed that the cracking initiated by fretting fatigue and propagated by cyclic shaft bending stresses. As part of a collaborative program Asea Brown Boveri (ABB) and Ontario Hydro undertook a material test program, described in this paper, to determine the near threshold fatigue crack propagation behaviour of the rotor material under service conditions. The effects of R-ratio ($\sigma_{min}/\sigma_{max}$), temperature and different gaseous environments on the threshold behaviour were investigated.

MATERIAL AND EXPERIMENTAL PROCEDURE

The generator rotor material, a quenched and tempered 3.5NiCrMoV steel, had a yield (0.2% offset) and ultimate strength of 751 and 855 MPa, respectively, at room temperature. Material tested at various locations through the thickness met all chemical and mechanical design specifications and indicated a good forging quality. Specimen were

* ABB Power Generation Ltd., Baden, Switzerland

** Metallurgical Research Department, Ontario Hydro Research Division, Toronto, Ontario, Canada

machined from the failed generator rotor and were oriented such that crack propagation was in the same orientation as the cracks in the failed rotor, that is, the radial-tangential plane. Double cantilever beam or CT specimen geometries were used for positive load ratio tests. Two different modified single edge notch (SEN) specimen geometries were used for negative load ratio tests. K_I calibrations were developed for the SEN specimens by finite element analysis using compliance measurements as appropriate boundary conditions.

The fatigue crack propagation tests and the determination of the threshold stress intensity factor range ΔK_{th} , were performed in accordance to ASTM E647-88 (1). In contrast to the ASTM definition ΔK was defined in the entire range of R-ratios as the difference between K_{max} , and K_{min} . Manual and automated methods were used to obtain the crack growth rate data. The crack length was determined by either the d.c. potential drop or the compliance technique and was verified by optical measurements. All tests were carried out on servo hydraulic machines at 30 Hz. Tests were conducted in (i) ambient air, (ii) hydrogen (99.99% H_2 , dew point below $-65^\circ C$, 0.5 MPa) and (iii) a simulated generator coolant gas (hydrogen with 500 ppm O_2 dew point $-20^\circ C$ at 0.5 MPa). The dew point was controlled by passing the water saturated gas through a coil chilled to $-20^\circ C$ before it was heated to the desired temperature in the test chamber (continuous flow).

RESULTS AND DISCUSSION

Crack Propagation at Positive R-Ratios

The effect of ambient air and pure hydrogen environments on ΔK_{th} are shown in Fig. 1 as a function of R-ratio. The values of ΔK_{th} in hydrogen are significantly lower than those in air at room temperature at lower R-ratios, but are similar to the ΔK_{th} values in air at room temperature at high R-ratios. In contrast to air, the R-ratio dependence of ΔK_{th} in hydrogen is much smaller: ΔK_{th} decreased marginally as the R-ratio increased from 0.1 to 0.9. Environmental effects of this type have been reported for NiCrMoV steel (2) and are attributed to the absence of oxide-induced crack closure. The fracture surfaces of the specimens tested in air exhibited a uniform brown-coloured oxide in the region close to the threshold. This layer was not visible on the fracture surfaces of the specimens tested in hydrogen. The presence of oxide films on the crack surfaces is known to increase the level of crack closure, thus increasing the apparent threshold values.

The influence of temperature on ΔK_{th} in air and hydrogen at an R-ratio of 0.1 is compared in Fig. 2 and 3. In air, the value of ΔK_{th} decreased as the temperature increased from $21^\circ C$ to $100^\circ C$. These results exhibit a trend similar to those reported for lower-strength CrMoV steel (3) and various pressure vessel steels (4) in which the reduction in ΔK_{th} over this temperature range was linked to a decrease in fracture surface roughness and roughness-induced crack closure. In

hydrogen, the effect of temperature on ΔK_{th} showed markedly different behaviour to that observed in air: the threshold values increased at elevated temperature, passing through a maximum at $60^\circ C$.

The near-threshold crack propagation behaviour in the various hydrogen environments are compared in Fig. 3 at a load ratio of 0.1. At $21^\circ C$, tests in water-saturated hydrogen or in dry hydrogen with an addition of 500 ppm oxygen showed no significant difference to that of the behaviour in dry hydrogen. At $100^\circ C$, the near-threshold crack growth rates in the moisture-containing simulated generator coolant were slightly lower than those in the dry hydrogen.

The fracture morphology consisted of a mixture of transgranular and intergranular fracture (Fig. 4). The fraction of intergranular fracture was dependent on the applied ΔK , R-ratio and environment. In air the percentage of intergranular fracture attained a maximum at $\Delta K=12 \text{ MPa}\sqrt{m}$ and decreased to zero at the threshold. The magnitude of this maximum decreased with increasing R-ratio. In hydrogen the proportion of intergranular fracture was greater than in air at ΔK values above the threshold. In all tests, the fracture morphology was transgranular at the threshold irrespective of the environment

Crack Propagation at Negative R-Ratios

The values of ΔK_{th} measured at $R=-1$ showed an unusually large variation (Fig.5). In the simulated generator hydrogen environment values of ΔK_{th} ranged from 7.4 to $12.2 \text{ MPa}\sqrt{m}$. The results appear to be related to the type of load shedding method used and how they in turn affected the surface roughness. Differences between the two load shedding methods are briefly described below:

- Procedure A (stepwise load shedding): specimen precracked in air at $R=0.1$ using low initial ΔK ; small increase in crack length until threshold was attained.
- Procedure B (continuous load shedding): specimen precracked in H, at $R=-1$ using high initial ΔK ; large increase in crack length until threshold was attained.

A lower value of ΔK_{th} was obtained using procedure B ($8.4 \text{ MPa}\sqrt{m}$ vs. $12.2 \text{ MPa}\sqrt{m}$ using procedure A, which was consistent with the features observed on the fracture surfaces. A higher degree of surface contact and deformation was evident on the fracture surface produced by procedure B. Regions of the crack surfaces having higher proportions of intergranular fracture exhibited a greater degree of plastic deformation than those produced by procedure A. Asperities in this region were markedly flattened by procedure B. More importantly, the region of transgranular fracture near the threshold showed a greater number of contact points with the mating fracture surface. These observations showed that procedure B produced a higher degree of surface flattening and indicate that a larger fraction of the compressive load was transferred closer

to the crack tip. In this manner, a lower level of crack closure likely existed, which resulted in a lower value of ΔK_{th} for procedure B. Two additional tests were carried out to clarify the mechanism causing the variation in ΔK_{th} at $R=-1$. In the first test procedure A was used to determine ΔK_{th} . However, immediately after fatigue precracking, and prior to the actual test, the specimen was subjected to tension-compression cycling at $R=-3.3$ ($K_{max}=6 \text{ MPa}\sqrt{\text{m}}$ for 2×10^6 cycles) This test yielded a value of $\Delta K_{th}= 7.4 \text{ MPa}\sqrt{\text{m}}$. In the second test the specimen was fatigue precracked according to procedure B. Crack closure levels were then monitored by a compliance-based method as the specimen was cycled at $R=-4$ ($K_{max}=3 \text{ MPa}\sqrt{\text{m}}$). During this load cycling no crack growth occurred and the closure load decreased from $0.42P_{max}$ to $0.28P_{min}$ after 5×10^5 cycles (Fig. 6).

The above results suggest that fatigue threshold values obtained at negative stress ratios can be influenced by the loading history. ΔK_{th} may not be unique for tests in which the fracture surfaces contain high percentage of intergranular fracture, which during compressive loading can be deformed into surfaces having a lower surface roughness. Under tension-compression loading fracture surfaces containing intergranular fracture can influence closure levels, and thus ΔK_{th} , by restraining the crack from fully closing. This type of behaviour can be expected because fracture surfaces behind the crack tip have been shown to influence closure levels (5,6).

DESIGN PERSPECTIVE

The data in Fig. 5 have practical consequences in defining non-destructive examination (NDE) requirements in rotor components. As the generator rotor has to be designed for infinite operating life the critical threshold flaw size must be greater than the NDE detectable flaw size. To calculate the critical threshold flaw size for the rotor steel the data in fig. 5 can be used to define a lower bound curve. At positive R-ratios the lower bound is given by the effective threshold value $\Delta K_{th,eff} = 2.8 \text{ MPa}\sqrt{\text{m}}$ (assuming no crack closure). At negative R-ratios $\Delta K_{th,eff}$ is multiplied by $(1-R)$ to account for the negative portion of the load cycle which does not contribute to crack growth. This lower bound curve and the critical threshold flaw size calculated from it can be applied to all service conditions, irrespective of R-ratio, temperature and environmental effects. This flaw size is compared with the detectable flaw size. For ultrasonic inspections the detectable flaw size depends on the shape and orientation of the flaw. If this information is not available the designer assumes a penny-shaped subsurface flaw oriented perpendicular to the shaft bending stress. The diameter of a critical threshold flaw determines the NDE detection limit in terms of a flat bottom hole (FBH) size. This approach, together with the lower bound threshold curve, will provide a truly conservative design limit.

A more realistic design limit can be established if the type of defect, its shape and orientation are known. In generator rotor forgings the flaws are cigar-shaped, have aspect ratios of up to 30, and are parallel to the rotor axis, i.e. parallel to the shaft bending stress. For this type of flaw the diameter determines the critical threshold flaw size. However, in contrast to the penny-shaped flaw the FBH value is not given by the diameter of the "cigar" but is equal to the diameter multiplied by the square root of the aspect ratio. Thus, for cigar-shaped flaws in generator rotor forgings, there is a considerable margin between critical threshold flaw size and detectable flaw size. The difference is proportional to the square root of the aspect ratio and can be as large as 5.5. This realistic approach indicates that the behaviour of real flaws is less critical than that of postulated pennys shaped flaws.

REFERENCES

1. ASTM Standard E647-88, Vol. 03.01, 1988.
2. Stewart, A.T., Eng. Fract. Mech., Vol. 13, 1980, pp 463-478.
3. Liaw, P.K., Saxena, A., Swaminathan, V.P. and Shih, T.T., Met. Trans. A., Vol. 14A, 1983, pp 1631-1640.
4. Liaw, P.K. and Logsdon, W.A., J. Eng. Mat. Tech., Vol. 107, 1985, pp 26-33.
5. Breat, J.L., Mundry, F. and Pineau, A., Fat. Engng. Mater. Struct., Vol. 6, 1983, pp 349-358.
6. Minakawa, K., Newman, Jr., J.C. and McEvily, A.J., Fat. Engng. Mater. Struct., Vol. 6, 1983, pp 359-365.

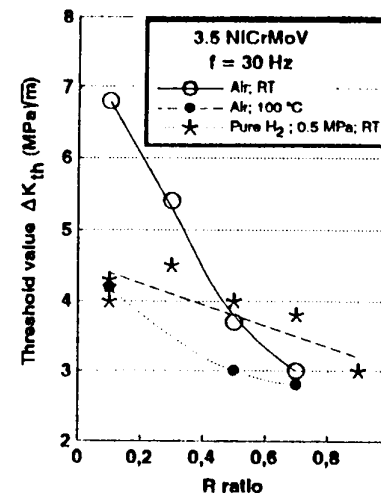


Fig.1 Comparison of ΔK_{th} in air and H_2

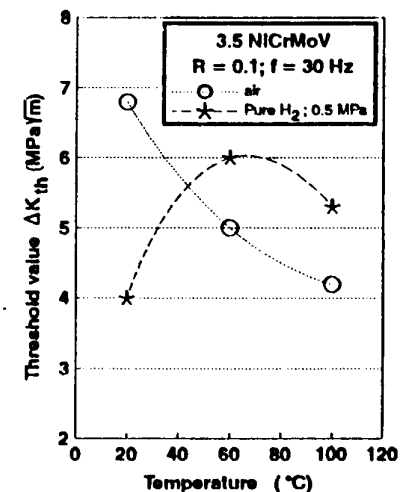


Fig.2 Effect of temperature on ΔK_{th} in air and H_2 at $R=0.1$

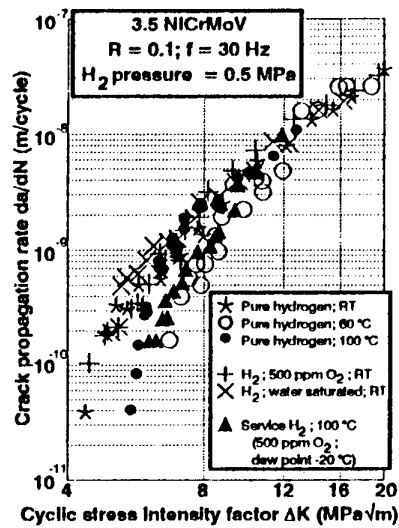


Fig.3 Effect of environment on crack growth rates at R=0.1

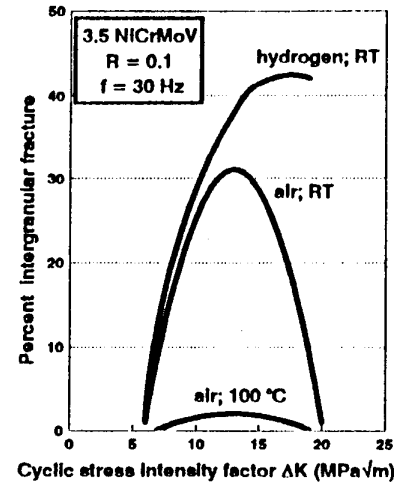


Fig.4 Intergranular fracture vs ΔK in air and H₂

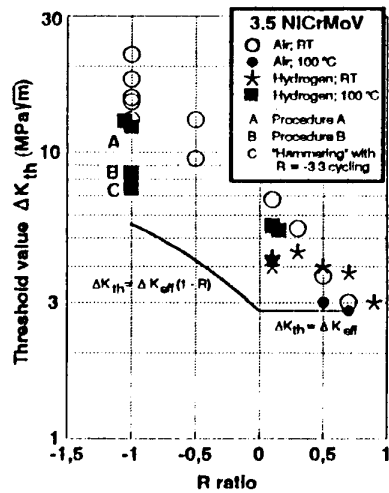


Fig.5 Effect of R-ratio on ΔK_{th}

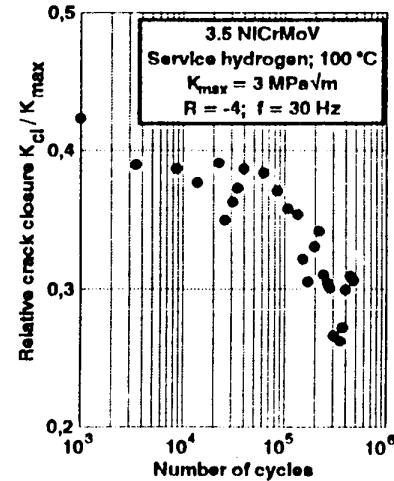


Fig.6 Effect of load cycling at R=-4 on closure levels